Inorganic Chemistry

pubs.acs.org/IC Article

Striking Improvement of N_2 Selectivity in NH_3 Oxidation Reaction on Fe_2O_3-Based Catalysts via SiO_2 Doping

Xiaoyu Ji, Bifeng Zhang, Huaizhu Wang, Yandi Cai, Qinglong Liu, Kaiqiang Wu, Dawei Li, Wei Tan,* Fudong Liu,* and Lin Dong

Cite This: https://doi.org/10.1021/acs.inorgchem.4c04482 Read Online

ACCESS | Metrics & More | Article Recommendations | Supporting Information

ABSTRACT: The emission of NH_3 has been reported to pose a serious threat to both human health and the environment. To efficiently eliminate NH_3, catalysts for the selective catalytic oxidation of NH_3 (NH_3−SCO) have been intensively studied. Fe_2O_3-based catalysts were found to exhibit superior NH_3 oxidation activity; however, the low N_2 selectivity made it less attractive in practical applications. In this work, aimed at improving the N_2 selectivity on Fe_2O_3-based catalysts, a simple SiO_2 doping strategy was proposed. Although the NH_3 oxidation activity showed almost no change on Fe_2O_3 after SiO_2 doping, the N_2 selectivity was significantly improved. Systematic characterizations revealed that SiO_2 doping could increase the specific surface area of Fe_2O_3, and a strong interaction of Fe−O−Si was formed in Fe_2O_3−SiO_2 mixed oxide catalysts. Furthermore, abundant Brønsted acid sites were formed on Fe_2O_3−SiO_2 catalysts due to the facile hydrolysis of the Fe−O−Si structure into Si−OH and Fe−OH. Although SiO_2 doping was found to weaken the redox ability of Fe_2O_3, the abundant Brønsted acid sites on Fe_2O_3−SiO_2 catalysts could facilitate NH_3 oxidation reaction through an internal SCR (*i*-SCR) pathway, thus achieving superior N_2 selectivity. This work can provide new insights into constructing efficient NH_3−SCO catalysts with high N_2 selectivity.

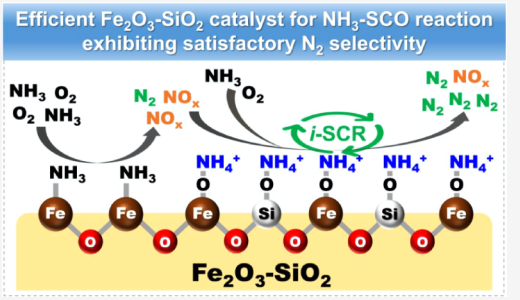

1. INTRODUCTION

Ammonia (NH_3) is one of the most important and commonly used chemicals for industrial production.[1,2] However, NH_3 slipping into the atmosphere can result in a series of environmental pollution problems (e.g., the formation of aerosols and $PM_{2.5}$ and water contamination).[2−5] Moreover, when the concentration of NH_3 in the air exceeds 300 ppm, NH_3 can pose an immediate threat to human health and even lead to death.[6−8] In recent decades, aimed at eliminating the NO_x emitted by both mobile and stationary sources, the selective catalytic reduction of NO_x by NH_3 (NH_3−SCR) technique has been widely applied, while excess NH_3 that is not consumed by NO_x and O_2 can also be emitted into the atmosphere, causing air pollution.[9−12] To deal with this problem, governments have enacted stringent regulations to control NH_3 slip.[13,14] As a result, it is urgent to develop efficient catalysts for the selective catalytic oxidation of NH_3 (NH_3−SCO) to harmless N_2 and H_2O (reaction (1)).[15] However, on most NH_3−SCO catalysts, the nonselective oxidation of NH_3 may also occur, especially at higher temperatures, thus generating NO, NO_2, and N_2O as byproducts (reactions (2), (3), and (4)).[16−18] To avoid the secondary pollution resulting from the byproducts, improving the N_2 selectivity has become one of the most focused hotspots for developing NH_3−SCO catalysts.

$$4NH_3 + 3O_2 \rightarrow 2N_2 + 6H_2O \quad (1)$$

$$4NH_3 + 5O_2 \rightarrow 4NO + 6H_2O \quad (2)$$

$$4NH_3 + 7O_2 \rightarrow 4NO_2 + 6H_2O \quad (3)$$

$$2NH_3 + 2O_2 \rightarrow N_2O + 3H_2O \quad (4)$$

Noble metal (e.g., Pt, Ir, and Ag) catalysts have been reported to exhibit excellent low-temperature activity in NH_3 oxidation reaction.[14,19,20] For example, Pt/Al_2O_3 catalysts have been industrially applied due to their satisfactory NH_3−SCO activity below 250 °C.[19,21] Wang et al. found that Ag supported on Al_2O_3 could also effectively catalyze the oxidation of NH_3 even at a low temperature of 100 °C.[22] However, it has to be noted that the facile activation of N−H on noble metal sites could always result in the severe deep oxidation of NH_3 to NO_x (NO, NO_2, or N_2O).[14,23,24] Although researchers have developed a variety of strategies, including tuning the dispersion or electronic states of noble metal species, using different supports and adjusting the strength of metal−support interactions, to improve the N_2

Received: October 21, 2024
Revised: December 24, 2024
Accepted: December 31, 2024

selectivity on noble metal catalysts in NH_3 oxidation reaction,[25−28] no desirable noble metal catalysts with superior NH_3 oxidation activity and N_2 selectivity at the same time have yet been developed. Considering the potential environmental risk of NO_x generated by the nonselective oxidation of NH_3, the possibility of developing NH_3−SCO catalysts with high N_2 selectivity based on transition metal materials has also raised the attention of researchers, even though the transition metal catalysts usually exhibit lower NH_3 oxidation activity than noble metal catalysts. Moreover, transition metal catalysts have a definite cost advantage over noble metal catalysts.

As one of the most abundant elements on earth, iron (Fe) and its oxides have been used intensively in catalysis field due to their superior redox performance, environmental friendliness, and low price.[1,29−31] In NH_3−SCO reaction, Fe_2O_3-based catalysts were reported to exhibit superior NH_3 oxidation activity and low N_2O formation; however, the N_2 selectivity was still far from satisfactory due to the generation of massive NO and NO_2.[32−34] Recently, it was disclosed that the formation of more Brønsted acid sites on Pt/Nb_2O_5 and Pd/Nb_2O_5 catalysts was conducive to improving the N_2 selectivity in NH_3−SCO reaction due to that the intermediates ($-NH_2$ and $-N_2H_4$) formed on Brønsted acid sites would be favorable for the formation of N_2.[35] Inspired by this, the construction of Brønsted acid sites on Fe_2O_3 materials could be an effective strategy to improve the N_2 selectivity for NH_3−SCO reaction on Fe_2O_3.

In this work, inspired by previous reports on SiO_2-modified Fe_2O_3 function materials,[36−41] a facile SiO_2 doping strategy was proposed to promote the N_2 selectivity in NH_3−SCO reaction on Fe_2O_3 catalysts. It was revealed that SiO_2 doping could significantly improve the N_2 selectivity and SO_2/H_2O resistance. Moreover, via systematic characterizations, the impact of SiO_2 doping on the crystal structure, redox performance, surface adsorption property of Fe_2O_3, and the reaction mechanism were investigated, which helped reveal the reasons for achieving superior N_2 selectivity on Fe_2O_3−SiO_2 catalysts in NH_3−SCO reaction.

2. EXPERIMENTAL SECTION

2.1. Catalysts Preparation. Fe_2O_3 and Fe_2O_3−SiO_2 catalysts were prepared by ethanol-assisted ammonia (co)-precipitation method, using ethanol as the solution and $NH_3\cdot H_2O$ (25%) as the precipitant. Analytically pure (AR) $Fe(NO_3)_3\cdot 9H_2O$ and tetraethyl orthosilicate (TEOS) were used as precursors. In detail, a certain amount of $Fe(NO_3)_3\cdot 9H_2O$ was dissolved in 200 mL ethanol under vigorous stirring. After the formation of a homogeneous solution, a specified proportion of TEOS was added dropwise, followed by 30 min of continuous stirring. Afterwards, excess $NH_3\cdot H_2O$ was dropped into the mixed solution until the pH reached 9. The obtained precipitate was aged overnight, washed three times with water, dried at 100 °C for 12 h, and finally calcined at 500 °C for 4 h with a ramping rate of 5 °C·min^{-1}. The prepared Fe_2O_3−SiO_2 mixed oxides were denoted as Fe*x*Si*y* (*x*:*y* was the molar ratio of $Fe(NO_3)_3\cdot 9H_2O$ and TEOS used in the preparation process). To evaluate the SO_2 resistance of the prepared catalysts, gas-phase sulfation treatment was conducted at 300 °C before catalytic performance evaluation. In sulfation treatment, 100 mg catalysts were loaded, and the feeding gas (100 mL·min^{-1}) was composed of 200 ppm SO_2 and 5% O_2, using Ar as balance. The sulfated catalysts were suffixed with -S.

Caution! *$NH_3\cdot H_2O$ (25%) is a liquid with a pungent odor and corrosive properties. All operations must be conducted in a fume hood.*

Caution! *Tetraethyl orthosilicate (TEOS) is extremely pyrophoric. This procedure controlled risk by the use of a very small amount of TEOS.*

2.2. Characterization. X-ray powder diffraction (XRD) patterns were collected on a LAB-X XRD-6000 diffractometer using Cu Kα radiation (0.15406 nm). The scan speed was 10°·min^{-1}, and the 2θ range was 10°−80° with a scan step of 0.02°.

Thermogravimetry (TG) analysis was carried out on a NETZSCH STA 449 F5 instrument. In each test, ca. 10 mg of catalyst was exposed to airflow and heated from 35 to 1000 °C linearly, with a ramping rate of 10 °C·min^{-1}.

Scanning electron microscopy (SEM) and elemental energy-dispersive spectroscopy (EDS) mapping images were collected on an FEI Nova Nano-450 instrument equipped with a Bruker QUANTAX accessory.

The specific surface area was measured on a Micromeritics ASAP-2020 analyzer using the Brunauer, Emmett, and Teller (BET) method. The pore volume and pore size distribution were calculated by the Barrett−Joyner−Halenda (BJH) method using desorption isotherms. To remove the impurities adsorbed on the surface of the samples, the samples were degassed at 300 °C for 4 h prior to testing.

X-ray fluorescence spectroscopy (XRF) experiments were conducted on an M4 Tornado instrument (Bruker Nano GmbH, Germany) equipped with a rhodium tube with a maximum excitation of 50 kV, 600 μA, and 30 W.

Attenuated total reflectance-Fourier transform infrared spectroscopy (ATR-FTIR) experiments were performed on a Nicolet iS50 FT-IR spectrometer equipped with an ATR accessory from 350 to 7800 cm^{-1}. Before the test, background spectra were collected at room temperature in air and subtracted from the recorded sample spectra in each test. The spectra were obtained by accumulating 100 scans with a resolution of 4 cm^{-1}.

H_2-temperature-programmed reduction (H_2-TPR) experiments were conducted on a quartz U-tube reactor connected to a thermal conductivity detector (TCD). Prior to the test, the loaded sample was first purged by N_2 flow (15 mL·min^{-1}) at 200 °C for 1 h. After cooling to room temperature, the pretreated sample was exposed to 7 vol % H_2/Ar flow (10 mL·min^{-1}) and heated to 870 °C linearly with a ramping rate of 10 °C·min^{-1}. The moisture in the outlet gas was removed by a cold trap, and the consumption of H_2 was monitored by the TCD.

X-ray photoelectron spectroscopy (XPS) experiments were performed on an ESCALAB QXi XPS system equipped with a monochromatic Al X-ray radiation source (1486.6 eV) with an accelerating power of 15 kW. The binding energies of all elements were calibrated with C 1s XPS peak at 284.6 eV.

NH_3-temperature-programmed desorption (NH_3-TPD) experiments were carried out on a fixed-bed quartz tubular microreactor. In each test, 100 mg catalyst was loaded into the quartz tube and purged by Ar flow (100 mL·min^{-1}) at 200 °C for 30 min. Then, the loaded catalyst was saturated with NH_3 after cooling to 50 °C and purged by Ar flow (100 mL·min^{-1}) to remove gaseous and weakly adsorbed NH_3. Finally, the catalyst was heated from 50 to 600 °C at a rate of 10 °C·min^{-1} in Ar flow (50 mL·min^{-1}). The concentration of NH_3 in the outlet gas was measured by an online Thermo Nicolet iS10

https://doi.org/10.1021/acs.inorgchem.4c04482
Inorg. Chem. XXXX, XXX, XXX−XXX

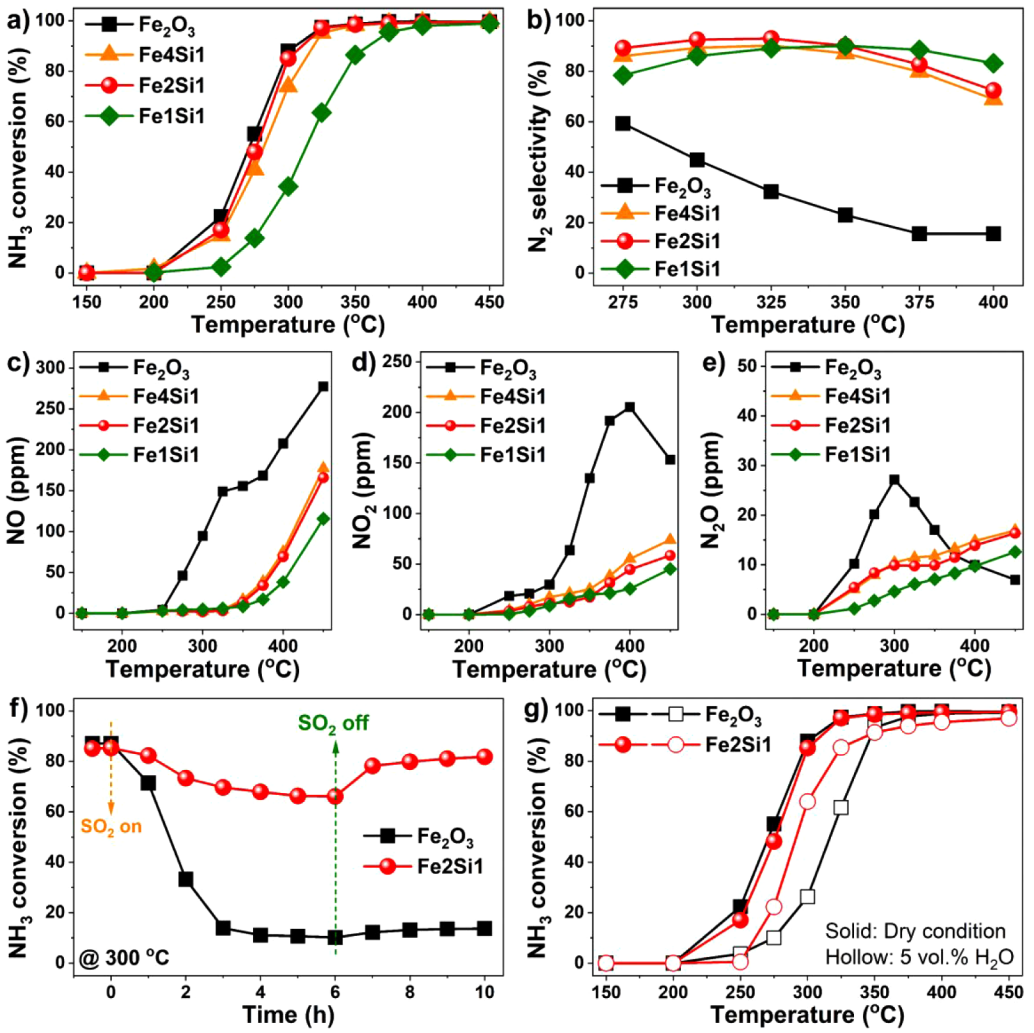

Figure 1. (a) NH_3 conversion and (b) N_2 selectivity on Fe_2O_3 and Fe*x*Si*y* in NH_3 oxidation reaction. The concentrations of (c) NO, (d) NO_2, and (e) N_2O generated on Fe_2O_3 and Fe*x*Si*y* in NH_3 oxidation reaction. (f) NH_3 conversion on Fe_2O_3 and Fe2Si1 in NH_3 oxidation reaction with the addition of 30 ppm SO_2 at 300 °C. (g) NH_3 oxidation activity on Fe_2O_3 and Fe2Si1 under dry and wet conditions. Reaction condition: 500 ppm NH_3, 5% O_2, 30 ppm SO_2 (when used), 5 vol % H_2O (when used), Ar as balance, WHSV = 60,000 mL·g^{-1}·h^{-1}.

Fourier transform infrared (FTIR) spectrometer equipped with a 2 m path-length gas cell.

In situ diffuse reflectance infrared Fourier transform spectroscopy (*in situ* DRIFTS) experiments were conducted on a Thermo Nicolet 5700 FTIR spectrometer, using a Mercury−Cadmium−Telluride (MCT) detector cooled by liquid N_2. The spectra were obtained by accumulating 32 scans with a resolution of 4 cm^{-1}. After being loaded into the DRIFTS cell, the samples were pretreated with air at 400 °C for 30 min to remove the adsorbed impurities. Then the background spectra were collected at the target temperature during the cooling process, which could be automatically subtracted from the sample spectra. In NH_3 adsorption, NH_3-TPD or NH_3 oxidation experiments, the feeding gas (50 mL·min^{-1}) contained 500 ppm NH_3 (when used) and 5% O_2 (when used), with N_2 as balance. The ramping rate for *in situ* DRIFTS of NH_3-TPD experiment was 10 °C·min^{-1}. In SO_2 + O_2 adsorption experiment, the feeding gas (100 mL·min^{-1}) was composed of 200 ppm SO_2 and 5% O_2, using N_2 as balance.

2.3. Catalytic Performance Evaluation. The catalytic performance evaluation was conducted on a fixed-bed quartz tubular microreactor using an online Thermo Nicolet iS10 FTIR spectrometer equipped with a 2 m path-length gas cell as a detector. All measurements were performed under a steady state. In a typical measurement of NH_3 oxidation activity, NH_3−SCR activity and N_2 selectivity, 100 mg catalyst was loaded and the feeding gas with a total flow rate of 100 mL·min^{-1} was composed of 500 ppm NH_3, 500 ppm NO (when used), and 5% O_2 (Ar as balance), giving a weight hourly space velocity (WHSV) of 60,000 mL h^{-1} g^{-1}. Due to the different densities of Fe_2O_3 and Fe2Si1, gas hourly space velocity (GHSV) for Fe_2O_3 and Fe2Si1 was 38,200 and 36,000 h^{-1}, respectively. For the kinetics study, the feeding gas was the same as that of the NH_3 oxidation activity and N_2 selectivity measurement. To eliminate the effects of mass and heat transfer, the loaded catalysts were mixed with SiC (mass ratio of catalyst to SiC = 1:10) and the amount of catalyst was varied in kinetic study to keep the NH_3 conversion below 20%.

The NH_3 conversion and N_2 selectivity in NH_3−SCO reaction were calculated using the following equations:

$$NH_3\text{conversion}(\%) = \frac{[NH_3]_{in} - [NH_3]_{out}}{[NH_3]_{in}} \times 100\%$$

https://doi.org/10.1021/acs.inorgchem.4c04482
Inorg. Chem. XXXX, XXX, XXX−XXX

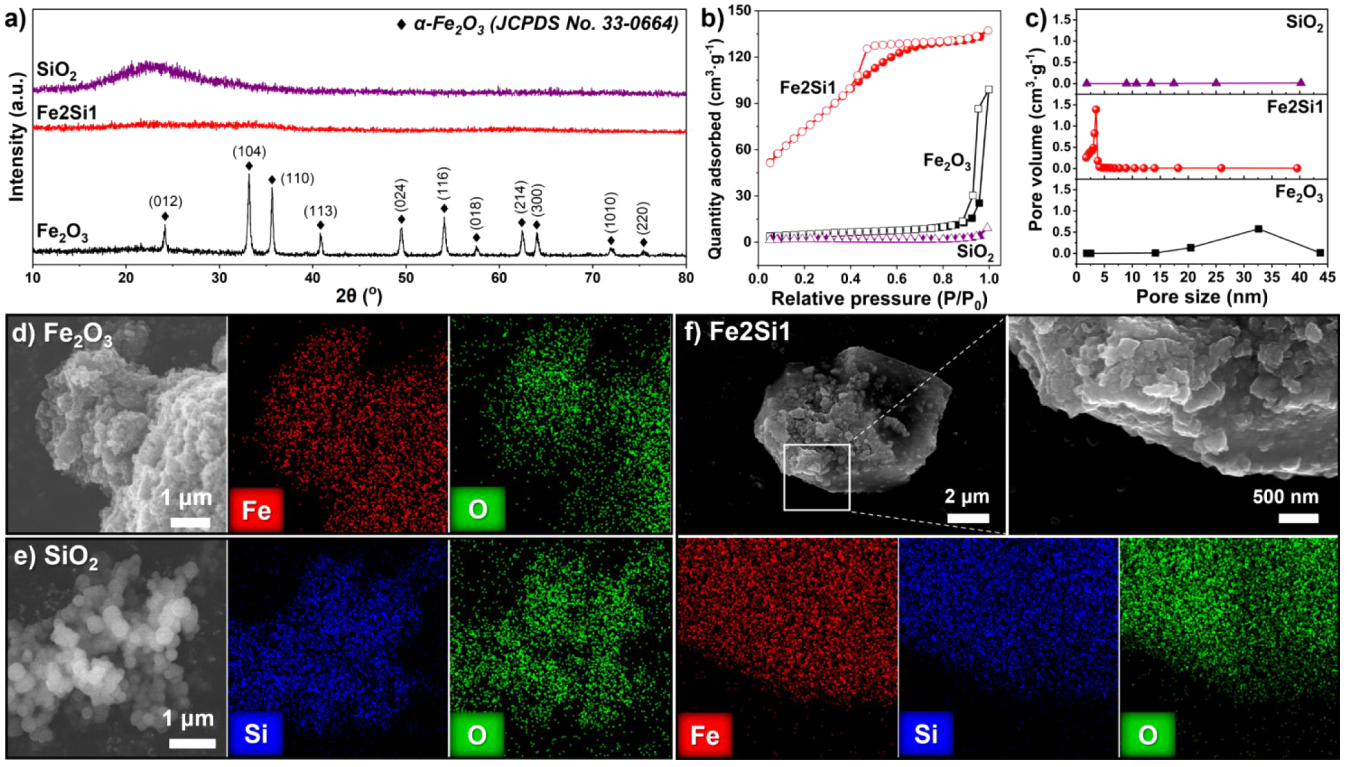

Figure 2. (a) XRD patterns, (b) Nitrogen adsorption−desorption isotherms and (c) BJH pore size distribution for Fe_2O_3, Fe2Si1 and SiO_2. SEM images and corresponding elemental EDS mapping images for (d) Fe_2O_3, (e) SiO_2 and (f) Fe2Si1.

$$N_2\ \text{selectivity}(\%) = \frac{[NH_3]_{in} - [NH_3]_{out} - [NO]_{out} - [NO_2]_{out} - 2[N_2O]_{out}}{[NH_3]_{in} - [NH_3]_{out}} \times 100\%$$

The NO conversion and N_2 selectivity in NH_3−SCR reaction were calculated using the following equations:

$$\text{NO conversion}(\%) = \frac{[NO]_{in} - [NO]_{out}}{[NO]_{in}} \times 100\%$$

$$N_2\ \text{selectivity}(\%) = \frac{[NH_3]_{in} + [NO]_{in} - [NH_3]_{out} - [NO]_{out} - [NO_2]_{out} - 2[N_2O]_{out}}{[NH_3]_{in} + [NO]_{in} - [NH_3]_{out} - [NO]_{out}} \times 100\%$$

3. RESULTS AND DISCUSSION

3.1. NH_3−SCO Catalytic Performance. NH_3 oxidation activity on Fe*x*Si*y* as a function of temperature is shown in Figure 1a. Fe4Si1 and Fe2Si1 showed comparable NH_3 oxidation activity to that of Fe_2O_3, on which the NH_3 conversion was higher than 95% above 325 °C. With the molar ratio of Fe to Si further decreased to 1:1, a slight decrease in the activity was observed. That is, Si doping could not contribute to the improvement of NH_3 oxidation activity on Fe_2O_3. Since N_2 selectivity was also an important performance indicator for NH_3−SCO catalysts, the N_2 selectivity on Fe_2O_3 and Fe*x*Si*y* was also calculated. As illustrated in Figure 1b, Fe_2O_3 showed rather low N_2 selectivity (<60%) at higher temperatures (>275 °C). Interestingly, the SiO_2 doping significantly improved the N_2 selectivity on Fe_2O_3, and Fe2Si1 exhibited the highest N_2 selectivity than Fe4Si1. For instance, the N_2 selectivity on Fe2Si1 (90%) at 350 °C was much higher than that on Fe_2O_3 (23%). The concentrations of NO, NO_2 and N_2O generated during the test are also plotted and shown in Figure 1c-e to demonstrate the effect of SiO_2 doping on the distribution of byproducts. SiO_2 doping was found to effectively inhibit the formation of NO, NO_2 and N_2O simultaneously, thus resulting in superior N_2 selectivity on Fe*x*Si*y*. When compared to those recently reported transition metal catalysts for NH_3−SCO reaction, Fe2Si1 still performed one of the best in terms of N_2 selectivity, especially at high temperatures (Table S1).

In the real application of emission control catalysts, SO_2 and H_2O in the exhaust might result in severe deactivation of catalysts. As a result, how to improve SO_2/H_2O resistance of catalysts has been a focus of attention in environment catalysis community. To investigate the SO_2 resistance of Fe_2O_3 and Fe2Si1, the SO_2 resistance of Fe_2O_3 and Fe2Si1 was evaluated by introducing 30 ppm SO_2 to the feeding gas at 300 °C. As shown in Figure 1f, although Fe_2O_3 and Fe2Si1 showed comparable NH_3 oxidation activity in the absence of SO_2, when SO_2 was introduced, NH_3 conversion on Fe2Si1 only showed a slight decrease from 85% to 65%, in clear contrast to the significant deactivation of Fe_2O_3, on which the NH_3 conversion decreased from about 88% to 10%. In addition, when SO_2 was turned off, the catalytic activity on Fe2Si1 would almost fully recover, while the activity on Fe_2O_3 only showed a limited increase. Additionally, N_2 selectivity on Fe_2O_3 was significantly improved after switching on SO_2 and kept at a high level even after turning off SO_2 (Figure S1). According to the previous report, it could be inferred that the deactivation of Fe sites (redox sites) and the improved surface acidity due to the formation of ferric sulfates accounted for the enhancement in the N_2 selectivity on Fe_2O_3.[42] This phenomenon also indicated that acid sites played a vital role in determining N_2 selectivity during NH_3 oxidation reaction.

https://doi.org/10.1021/acs.inorgchem.4c04482
Inorg. Chem. XXXX, XXX, XXX−XXX

To further investigate the effect of SO_2 on the catalytic performance of Fe_2O_3 and Fe2Si1, NH_3 oxidation activity and N_2 selectivity on presulfated catalysts were also measured. As demonstrated in Figure S2a, NH_3 oxidation activity on Fe_2O_3 decreased dramatically after sulfation treatment, with T_{50} (the temperature at which NH_3 conversion reached 50%) increasing from 267 to 363 °C. Surprisingly, the poisoning effect of sulfation on Fe2Si1 was much milder, with a limited increase in T_{50} of *ca.* 30 °C. In addition, improved N_2 selectivity was achieved on sulfated catalysts (Figure S2b,c). According to the results of *in situ* DRIFTS of SO_2 + O_2 adsorption and TG experiments (Figure S3), the better SO_2 resistance of Fe2Si1 was due to the fact that Si doping could effectively inhibit SO_2 adsorption on Fe_2O_3. That is, SiO_2 doping is indeed an effective strategy for alleviating SO_2 poisoning of Fe_2O_3 in NH_3−SCO reaction. Moreover, although Cu and Mn-based catalysts have been reported to exhibit superior NH_3 oxidation activity, Fe2Si1 was advantageous to them in terms of SO_2 resistance.[43] The NH_3 oxidation activity on Fe_2O_3 and Fe2Si1 was also evaluated under wet conditions (5 vol % H_2O) to investigate the effect of H_2O. It was found that Fe2Si1 still exhibited higher NH_3 oxidation activity (Figure 1g) and N_2 selectivity (Figure S4) than Fe_2O_3 in the presence of H_2O. Although N_2 selectivity on Fe2Si1 was improved in the presence of H_2O, N_2 selectivity on Fe_2O_3 decreased significantly. It was noteworthy that more NO was formed on Fe_2O_3 under wet conditions (Figure S5), which should be the main reason for its lower N_2 selectivity. According to the previous report, −OH species derived from adsorbed H_2O could promote the generation of NO from −HNO species (−HNO + −OH → NO + H_2O).[44] The lower NH_3 conversion as well as the formation of more NO well accounted for the decreased N_2 selectivity on Fe_2O_3.

In short summary, although SiO_2 doping did not contribute to the improvement of NH_3 oxidation activity on Fe_2O_3, the drastic enhancement in the N_2 selectivity as well as SO_2/H_2O resistance was achieved on Fe2Si1.

3.2. Structural Properties. XRD patterns for Fe_2O_3 and Fe2Si1 were first collected to investigate the possible differences in their crystal structure. As shown in Figure 2a, all well-defined diffraction peaks on Fe_2O_3 could be assigned to hematite (JCPDS#33−0664). In clear contrast, no identifiable diffraction peak was observed on Fe2Si1, implying that amorphous Fe_2O_3−SiO_2 mixed oxide was successfully synthesized by a facile coprecipitation method, and Fe_2O_3 and SiO_2 might be highly mixed. Raman spectra (Figure S6) further proved that SiO_2 doping could significantly effectively decrease the crystallinity of Fe_2O_3. Moreover, according to the results of SEM and elemental EDS mapping (Figure 2d-f), Fe_2O_3, SiO_2 and Fe2Si1 were in irregular morphology, and the distribution of Si in Fe2Si1 matched well with that of Fe, confirming that uniform Fe_2O_3−SiO_2 mixed oxides with low crystallinity were successfully synthesized by ethanol-assisted ammonia (co)precipitation method. The unique function of SiO_2 doping in decreasing the crystallinity of Fe_2O_3 could be explained from the perspective of the TEOS hydrolysis process. Since the hydrolysis of TEOS and the condensation of silicic acid could easily occur under acidic conditions, H^+ (H_3O^+) or C_2H_5−OH_2^+ generated in the ethanol solution of $Fe(NO_3)_3{\cdot}9H_2O$ could induce the hydrolysis of TEOS and the formation of $SiO_x(OH)_y$ before the addition of $NH_3{\cdot}H_2O$. As a result, $SiO_x(OH)_y$ framework in ethanol solution could retard the growth of $Fe(OH)_3$ cores and adsorb $Fe(OH)_3$ particles after the addition of $NH_3{\cdot}H_2O$. Besides, the interaction between Si and Fe through bridging oxygen was formed during the subsequent drying and calcination processes, thus further inhibiting the crystallization of Fe_2O_3. N_2-physisorption was also conducted on Fe_2O_3 and Fe2Si1 to further understand their structure. As shown in Figure 2b, Fe_2O_3 and SiO_2 exhibited type IV isotherms with H3 hysteresis loops, indicating their mesoporous structure.[45] Differently, Fe2Si1 showed type IV isotherms with H2 hysteresis loops, demonstrating the formation of tubular mesopores.[46] Moreover, it was also found that abundant mesopores with a uniform pore size of *ca.* 3.5 nm were formed on Fe2Si1 (Figure 2c), indicating the formation of regular mesoporous structure in Fe2Si1, which also well explained that Fe2Si1 (272 $m^2{\cdot}g^{-1}$) showed the much higher specific surface area than Fe_2O_3 (17 $m^2{\cdot}g^{-1}$) (Table 1). The high specific surface area of Fe*x*Si*y* with different Fe−Si ratios (Table S2) confirmed that Si doping is an effective and reproducible strategy for increasing the specific surface area of Fe_2O_3. The significantly decreased crystallinity and remarkable increase in the specific surface area of Fe_2O_3 after SiO_2 doping also hinted at the formation of a unique strong interaction between Fe and Si. The composition of Fe2Si1 was measured by XRF and is listed in Table 1. The real molar ratio of Fe:Si in Fe2Si1 determined by XRF (4.3:1) was higher than the theoretical value (2:1), which could be due to incomplete condensation of silicic acid under alkaline conditions. However, as shown in Table S2, the addition of more TEOS still led to a corresponding decrease in the molar ratio of Fe:Si. When the amount of Fe_2O_3 was reduced to the equivalent amount of Fe_2O_3 in Fe2Si1 in catalytic performance evaluation based on the results of XRF, NH_3 conversion on Fe_2O_3 slightly decreased as expected (Figure S7), but it was still comparable to that on Fe2Si1, confirming that the primary role of Si doping is to enhance the N_2 selectivity and SO_2/H_2O resistance of the catalysts.

Table 1. Results of N_2 Physisorption and XRF

Samples	S_{BET}($m^2{\cdot}g^{-1}$)[a]	Pore volume ($cm^3{\cdot}g^{-1}$)[b]	n_{Fe}:n_{Si}[c]
Fe_2O_3	17	0.15	-
Fe2Si1	272	0.21	4.3:1
SiO_2	6	0.01	-

[a]S_{BET} meant the specific surface area of catalysts calculated by BET method using desorption isotherms. [b]The pore volume was determined by BJH method using desorption isotherms. [c]n_{Fe}:n_{Si} meant the molar ratio of Fe to Si in Fe2Si1 catalysts determined by XRF.

3.3. The Interaction between Fe and Si. To further investigate the surface structure of Fe2Si1 and the possible interaction between Fe and Si, ATR-FTIR experiment was performed. As demonstrated in Figure 3a, for SiO_2, the bands at 961 and 1073 cm^{-1} were related to Si−OH and Si−O−Si, respectively.[47−49] After Si doping, bands at lower wavenumbers were observed. The band at 1007 cm^{-1} could be attributed to the vibration of Fe−O−Si structure, and the band centered at 906 cm^{-1} was related to the mixture of IR bands attributed to Fe−OH or Si−OH species, suggesting the formation of Fe−O−Si and Fe−OH/Si−OH structures in Fe2Si1.[50,51] Moreover, the more intensive broad band at 2700−3600 cm^{-1} on Fe2Si1 than that on Fe_2O_3 and SiO_2 should be due to the formation of more surface hydroxyl groups (Si−OH and Fe−

https://doi.org/10.1021/acs.inorgchem.4c04482
Inorg. Chem. XXXX, XXX, XXX−XXX

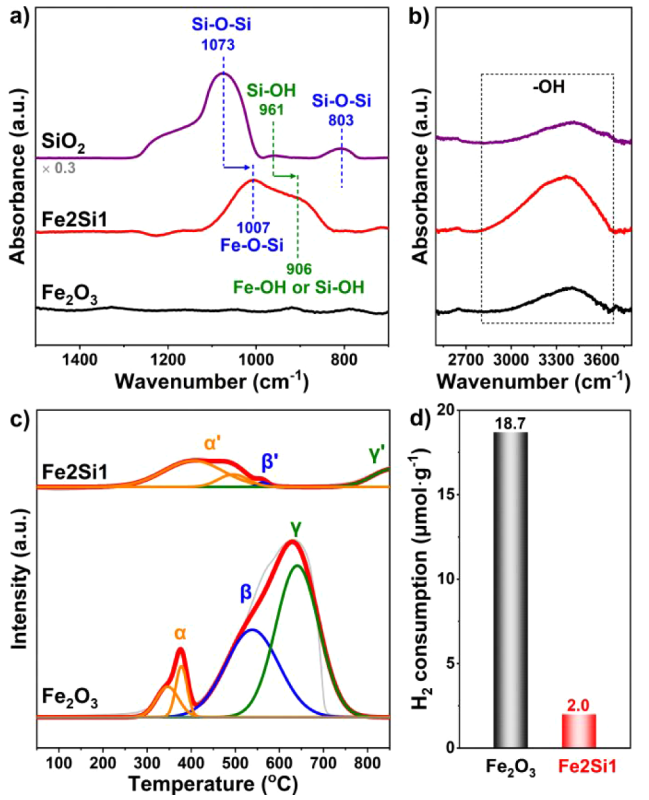

Figure 3. (a, b) ATR-FTIR spectra of Fe_2O_3 and Fe2Si1 catalysts. (c) H_2-TPR profiles for Fe_2O_3 and Fe2Si1. (d) The total consumption of H_2 for Fe_2O_3 and Fe2Si1.

OH) on Fe2Si1 generated by the flexible hydrolysis of Fe−O−Si structure (Figure 3b).[49]

Besides being used to evaluate the redox performance of catalysts, H_2-TPR technique has also been taken as a powerful tool for probing the interaction between different components in a catalyst. As shown in Figure 3c, three main H_2-consumption peaks were observed on Fe_2O_3 from low to high temperatures, which could be attributed to the reduction of Fe_2O_3 to Fe_3O_4 (peak α, marked as orange), the reduction of Fe_3O_4 to FeO (peak β, marked as blue) and the reduction of FeO to Fe (peak γ, marked as green), respectively.[52] Interestingly, after SiO_2 doping, the H_2-consumption peak attributed to the reduction of Fe_2O_3 to Fe_3O_4 (peak α') shifted to higher temperatures from 379 to 415 °C, and H_2-consumption peaks related to the reduction of Fe_3O_4 (peak β') and FeO (peak γ') on Fe2Si1 were much weaker than peak β and peak γ on Fe_2O_3, which could be due to the fact that the strong interaction between Fe and Si substantially inhibited the reduction of $Fe^{\delta+}$ to Fe with lower valence. That is, SiO_2 doping weakened the redox performance of Fe_2O_3, which could then suppress the potential deep oxidation of NH_3 to NO_x.[53] The total H_2 consumption of Fe_2O_3 and Fe2Si1 was also calculated and shown in Figure 3d. Since the reduction of $Fe^{\delta+}$ would be significantly inhibited by Si doping, the difference between the theoretical and actual hydrogen consumption amount (ΔH_2) of Fe*x*Si*y* should be positively related to the amount of Fe−O−Si structure. The theoretical H_2 consumption amount was calculated based on the content of Fe_2O_3 in Fe*x*Si*y* catalysts. As shown in Figure S8, with the Fe−Si ratio increased from 1:1 to 4:1, it was found that ΔH_2 increased first and then decreased, indicating that the amount of Fe−O−Si structure in Fe*x*Si*y* showed a volcano plot with the increase of Fe ratio, and the highest amount of Fe−O−Si structure was achieved on Fe2Si1.

To further understand the surface chemical states of Fe2Si1, XPS experiments were conducted. As shown in Figure 4a,b,

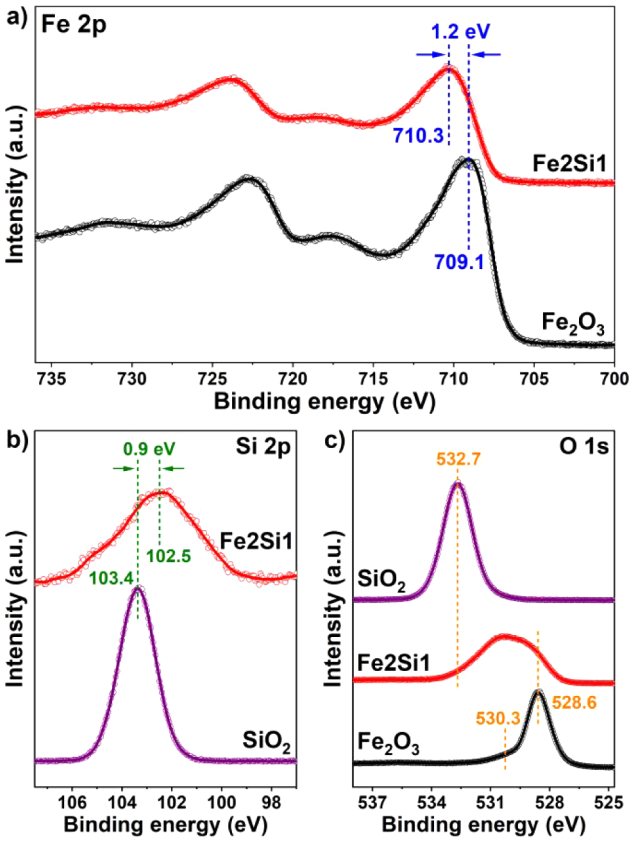

Figure 4. (a) Fe 2p XPS for Fe_2O_3 and Fe2Si1; (b) Si 2p XPS for SiO_2 and Fe2Si1; (c) O 1s XPS for Fe_2O_3, Fe2Si1 and SiO_2.

after the doping of SiO_2, Fe 2p XPS for Fe_2O_3 shifted to higher binding energy while Si 2p XPS shifted to lower binding energy. Such remarkable shifts indicated the electron transfer between Fe and Si atoms. That is, a strong interaction between Fe and Si was formed on Fe2Si1 catalyst. O 1s XPS for Fe_2O_3, Fe2Si1, and SiO_2 were also collected and shown in Figure 4c. The peaks at 528.6 and 530.3 eV on Fe_2O_3 could be attributed to lattice oxygen species and surface oxygen species, respectively.[54] A highly symmetrical peak at 532.7 eV was observed on the SiO_2. Completely different from the results of the O 1s XPS for Fe_2O_3, SiO_2 or the simple mixture of these two, the O 1s XPS peak on Fe2Si1 showed a broader peak shape and was located between the O 1s XPS peaks on Fe_2O_3 and SiO_2. Based on this, it could be inferred that this unique O 1s XPS peak on Fe2Si1 should be related to the oxygen atom in the Fe−O−Si structure.

In short summary, the results of ATR-FTIR, H_2-TPR, and XPS indicated that a strong interaction between Fe and Si was formed in the Fe2Si1 catalyst through the Fe−O−Si structure, which accounted for its unique textural property and redox performance.

3.4. Surface Adsorption Property and Reaction Mechanism. The adsorption of NH_3 on the catalyst is the first step of NH_3 oxidation reaction, which could significantly determine the catalytic performance.[8,55,56] In order to

https://doi.org/10.1021/acs.inorgchem.4c04482
Inorg. Chem. XXXX, XXX, XXX−XXX

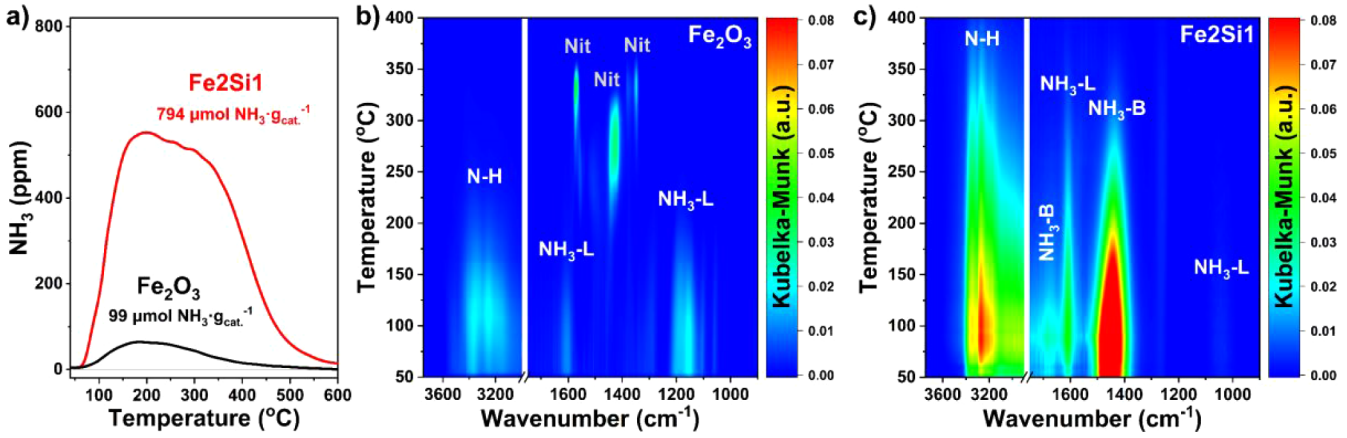

Figure 5. (a) NH_3-TPD profiles for Fe_2O_3 and Fe2Si1. *In situ* DRIFTS of NH_3-TPD on (b) Fe_2O_3, and (c) Fe2Si1.

investigate the NH_3 adsorption−desorption process on Fe_2O_3 and Fe2Si1, NH_3-TPD experiments were carried out. As shown in Figures 5a and S9, the NH_3-desorption peaks on Fe2Si1 were much more intensive than those on Fe_2O_3, and rather limited NO_x was generated during the desorption process, which meant that more NH_3 adsorption sites (acid sites) were formed on Fe2Si1. Further peak fitting analysis suggested that the total NH_3 adsorption amount on Fe2Si1 (794 μmol $NH_3 \cdot g_{cat.}^{-1}$) was 7 times that on Fe_2O_3 (99 μmol $NH_3 \cdot g_{cat.}^{-1}$), suggesting that SiO_2 doping could significantly facilitate the formation of acid sites on Fe_2O_3 catalysts.

To identify the types of acid sites on Fe_2O_3 and Fe2Si1 and determine the acidity strength of different acid sites, *in situ* DRIFTS of NH_3-TPD experiments were also conducted (Figure 5b,c). It was found that the acid sites on Fe_2O_3 were mainly in the form of Lewis acid sites (1175 and 1605 cm^{-1}, marked as NH_3-L), while the IR bands attributed to NH_3 species adsorbed on both Lewis acid sites (1605 cm^{-1}) and Brønsted acid sites (1435 and 1680 cm^{-1}, marked as NH_3−B) were observed on Fe2Si1.[57−63] Considering the drastic increase in the amount of surface acid sites on Fe2Si1, it could be concluded that SiO_2 doping could effectively induce the generation of abundant Brønsted acid sites on Fe_2O_3. As discussed in ATR-FTIR section, more hydroxyl groups were formed on Fe2Si1 due to the flexible hydrolysis of Fe−O−Si structure and the resulting Fe−OH and Si−OH species, and those hydroxyl groups could serve as Brønsted acid sites. Furthermore, NH_3 adsorbed on Fe_2O_3 could desorb at lower temperatures when compared to that adsorbed on Fe2Si1, suggesting that the Brønsted acid sites and Lewis acid sites on Fe2Si1 showed stronger acidity than those on Fe_2O_3. Interestingly, although O_2 was not introduced to the DRIFTS cell throughout the NH_3 desorption process, obvious bands attributed to nitrates (1350, 1420, and 1570 cm^{-1}, marked as Nit) were observed on Fe_2O_3 (≥ 200 °C), implying that oxygen species on Fe_2O_3 were highly reactive to NH_3, well explaining that Fe_2O_3 still exhibited slightly higher NH_3 oxidation activity than Fe2Si1 at low temperatures even with much fewer acid sites (Figure 1a).[64−66] However, the efficient nonselective oxidation of NH_3 to NO_x on Fe_2O_3 might also result in the decrease of N_2 selectivity. The more facile activation of NH_3 and O_2 on Fe_2O_3 could be further confirmed by the lower apparent activation energy (E_a) on Fe_2O_3 (99 kJ·mol^{-1}) than that on Fe2Si1 (165 kJ·mol^{-1}), as illustrated in Figure 6. More interestingly, although E_a on Fe2Si1 was higher

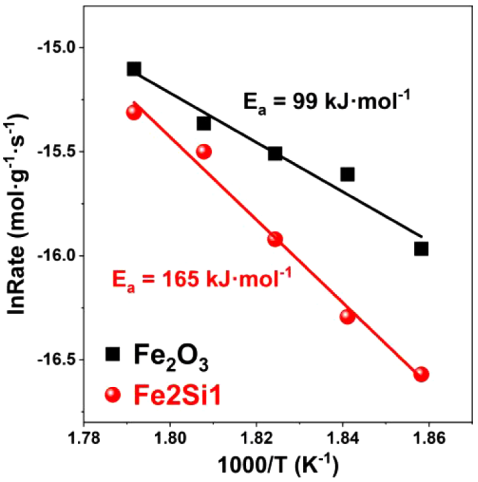

Figure 6. Arrhenius plots and apparent activation energy (E_a) values for NH_3 oxidation on Fe_2O_3 and Fe2Si1.

than that on Fe_2O_3 in NH_3 oxidation reaction, the activity on Fe_2O_3 and Fe2Si1 was quite close at relatively high temperature (> 275 °C), which could be resulted from the formation of more acid sites on Fe2Si1 and the different reaction pathways on these two catalysts. When normalizing the reaction rate by specific surface area (Figure S10), Fe_2O_3 was found to show a much higher NH_3 oxidation reaction rate per unit surface area than Fe2Si1, which could be due to the weakened redox capability of Fe_2O_3 after Si doping.

It has been widely recognized that reaction mechanisms on NH_3−SCO catalysts had a significant impact on their catalytic activity and N_2 selectivity.[67,68] To reveal the reasons for the different N_2 selectivity on Fe_2O_3 and Fe2Si1 from a reaction mechanism perspective, *in situ* DRIFTS of NH_3 adsorption and NH_3 oxidation experiments were conducted at 275 °C. As shown in Figure 7a, for Fe_2O_3, the band at 1190 cm^{-1} could be attributed to NH_3 adsorbed on Lewis acid sites (NH_3-L) and the peaks at 3133, 3221, and 3348 cm^{-1} were related to N−H stretching vibration modes.[54,69−73] The negative bands at 1227 and 1275 cm^{-1} should be related to the consumption of surface groups due to NH_3 adsorption. Furthermore, the absence of intensive bands at *ca.* 1440 cm^{-1} further confirmed that limited Brønsted acid sites were formed on Fe_2O_3, in good consistency with the results of *in situ* DRIFTS of NH_3-TPD.[74] Upon the introduction of O_2 into the feeding gas, it could be

https://doi.org/10.1021/acs.inorgchem.4c04482
Inorg. Chem. XXXX, XXX, XXX−XXX

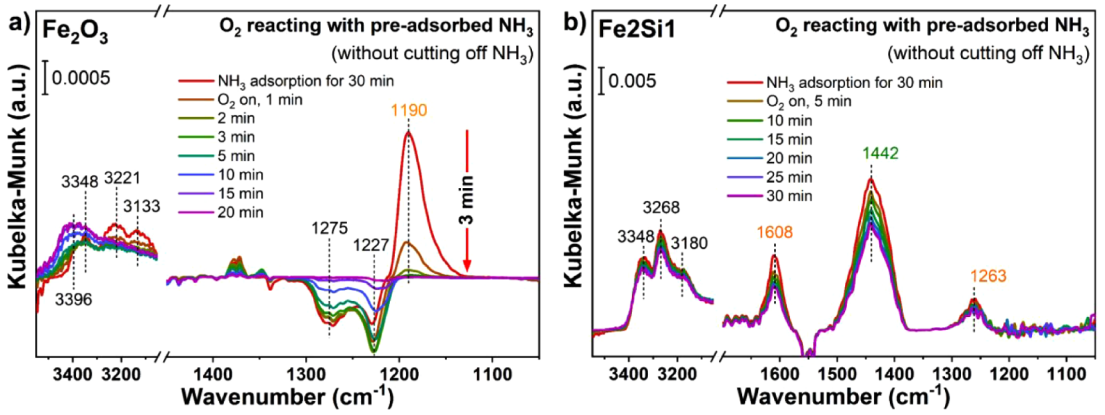

Figure 7. *In situ* DRIFTS of NH_3 adsorption and NH_3 oxidation on (a) Fe_2O_3 and (b) Fe2Si1 at 275 °C.

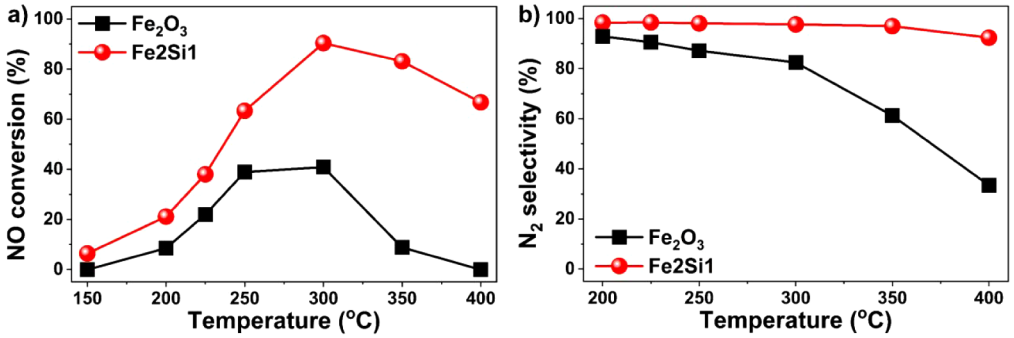

Figure 8. (a) NO conversion and (b) N_2 selectivity on Fe_2O_3 and Fe2Si1 catalysts in NH_3−SCR reaction.

observed that the intensity of the bands related to NH_3-L species decreased rapidly, and NH_3-L species (1190 cm^{-1}) were hardly observed after 3 min, indicating that NH_3-L species on Fe_2O_3 was highly reactive to O_2. Based on the results of catalytic performance evaluation (Figure 1), it can be concluded that NH_3 adsorption on Lewis acid sites (FeO_x species) could contribute to the enhancement of NH_3 oxidation activity and might play a negative role in N_2 selectivity, which was consistent with previous reports.[75,76] After the introduction of O_2 for 20 min, the negative bands at 1227 and 1275 cm^{-1} disappeared, which further confirmed that those two bands should be resulted from the consumption of surface oxygen species during the adsorption of NH_3. The formation of the intensive band at 3396 cm^{-1} could be related to the generation of surface hydroxyl groups during the oxidation of NH_3.[49] For Fe2Si1, besides the bands related to NH_3-L species (1263 and 1608 cm^{-1}), intensive band ascribed to NH_4^+ species coordinated to Brønsted acid sites (1441 cm^{-1}) was also observed on Fe2Si1 (Figure 7b), which meant that Si doping could help the generation of more acid sites with strong acid strength on Fe_2O_3, which were mainly in the form of Brønsted acid sites (Si−OH and Fe−OH).[77−79] It was observed that both NH_3-L and NH_3−B species on Fe2Si1 were consumed by O_2, and equilibrium was achieved in 30 min. Interestingly, unlike that bands related to NH_3-L species could be hardly observed on Fe_2O_3 a few minutes after the introduction of O_2, NH_3-L species still could be clearly observed on Fe2Si1, suggesting that NH_3-L species on Fe2Si1 were less reactive than those on Fe_2O_3, which could be due to the inferior redox performance of Fe sites strongly interacting with Si. Considering that Fe2Si1 exhibited a higher N_2 selectivity, abundant Brønsted acid sites on Fe2Si1 might play a more prominent role in improving N_2 selectivity. Specifically, the reaction between NO_x generated on FeO_x sites (Lewis acid sites) and NH_3 adsorbed on Brønsted acid sites (Fe−OH/Si−OH) was the key step in improving the N_2 selectivity.

Although the bands attributed to adsorbed nitrites/nitrates were not observed on both Fe_2O_3 and Fe2Si1 due to the weak adsorption strength and the fast reaction between gaseous NO_x and NH_3, it still could be deduced from the results of catalytic performance evaluation and *in situ* DRIFTS of NH_3 oxidation that the presence of abundant NH_4^+ species (NH_3−B) existed on Fe2Si1 under reaction condition might better facilitate the conversion of gaseous NO_x to N_2 through the internal selective catalytic reduction (*i*-SCR) pathway if part of NH_3 has been nonselectively oxidized to NO_x. For Fe_2O_3, the relatively better redox performance as suggested by H_2-TPR experiments, and much fewer remaining adsorbed NH_3 species on it under reaction conditions were unfavorable for the *i*-SCR pathway, thus resulting in the lower N_2 selectivity.

To support our viewpoint that Fe2Si1 catalyst could benefit the elimination of NO_x generated by nonselectivity oxidation of NH_3 through *i*-SCR pathway, NH_3−SCR activity on Fe2Si1 and Fe_2O_3 was also evaluated. As shown in Figure 8a, although Fe2Si1 showed slightly lower NH_3 oxidation activity than Fe_2O_3, much better NH_3−SCR activity was achieved on Fe2Si1, which meant that NH_3 adsorbed on Fe2Si1 showed higher reactivity to NO. That is, NO_x generated by nonselective oxidation of NH_3 on Fe2Si1 could be effectively consumed by adsorbed NH_3 through *i*-SCR reaction pathway, which also well explained the much lower concentration of NO_x generated on Fe2Si1 from 250 to 400 °C in NH_3 oxidation reaction (Figure 1c-e). Moreover, Fe2Si1 also

https://doi.org/10.1021/acs.inorgchem.4c04482
Inorg. Chem. XXXX, XXX, XXX−XXX

showed higher N_2 selectivity than Fe_2O_3 in NH_3−SCR reaction (Figure 8b), further confirming that Si doping could suppress the nonselective oxidation of NH_3 on Fe_2O_3. To facilitate understanding, a possible reaction pathway of NH_3 oxidation reaction on Fe2Si1 was proposed and shown in Scheme 1.

Scheme 1. A Proposed NH_3 Oxidation Reaction Pathway on Fe2Si1

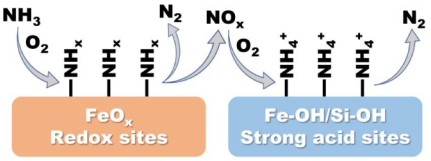

4. CONCLUSIONS

In order to improve the N_2 selectivity in NH_3−SCO reaction on Fe_2O_3 catalysts, a facile strategy of SiO_2 doping was proposed in this work. Through an ethanol-assisted ammonia coprecipitation method, amorphous Fe_2O_3−SiO_2 mixed oxides were successfully prepared, with the formation of the Fe−O−Si interaction. Due to the higher surface area and the more abundant surface hydroxyl groups (Fe−OH and Si−OH), Fe2Si1 possessed more acid sites than Fe_2O_3, and these acid sites were mainly in the form of Brønsted acid sites. Although the redox performance of Fe_2O_3 was weakened by SiO_2 doping due to the Fe−O−Si interaction leading to a decrease in the ability to activate NH_3, the higher concentration of surface acid sites on Fe2Si1 could effectively compensate for the relatively weak redox performance. Moreover, it was revealed that the abundant Brønsted acid sites on Fe2Si1 could induce the reaction between NH_4^+ and NO_x generated by the deep oxidation of NH_3 through an *i*-SCR pathway, which could further decrease the concentration of NO_x in the final products. This work paved a new way for developing NH_3−SCO catalysts with superior N_2 selectivity.

■ ASSOCIATED CONTENT

Supporting Information

The Supporting Information is available free of charge at https://pubs.acs.org/doi/10.1021/acs.inorgchem.4c04482.

Catalytic performance of reference catalysts, N_2-physisorption, NH_3 oxidation activity, N_2 selectivity, SO_2+O_2-DRIFTS, TG, Raman spectra, H_2-TPR, NH_3-TPD, kinetic study (PDF)

■ AUTHOR INFORMATION

Corresponding Authors

Wei Tan − *State Key Laboratory of Pollution Control and Resource Reuse, School of Environment, Jiangsu Key Laboratory of Vehicle Emissions Control, Center of Modern Analysis, Key Laboratory of Mesoscopic Chemistry of MOE, School of Chemistry and Chemical Engineering, Nanjing University, Nanjing 210023, China;* orcid.org/0000-0002-1481-9346; Email: tanwei@nju.edu.cn

Fudong Liu − *Department of Chemical and Environmental Engineering, Bourns College of Engineering, Center for Environmental Research and Technology (CE-CERT), Materials Science and Engineering (MSE) Program, University of California, Riverside, California 92521, United States;* orcid.org/0000-0001-8771-5938; Email: fudong.liu@ucr.edu, lfd1982@gmail.com

Authors

Xiaoyu Ji − *State Key Laboratory of Pollution Control and Resource Reuse, School of Environment, Jiangsu Key Laboratory of Vehicle Emissions Control, Center of Modern Analysis, Key Laboratory of Mesoscopic Chemistry of MOE, School of Chemistry and Chemical Engineering, Nanjing University, Nanjing 210023, China*

Bifeng Zhang − *State Key Laboratory of Pollution Control and Resource Reuse, School of Environment, Jiangsu Key Laboratory of Vehicle Emissions Control, Center of Modern Analysis, Key Laboratory of Mesoscopic Chemistry of MOE, School of Chemistry and Chemical Engineering, Nanjing University, Nanjing 210023, China*

Huaizhu Wang − *State Key Laboratory of Coordination Chemistry, MOE Key Laboratory of Mesoscopic Chemistry, MOE Key Laboratory of High Performance Polymer Materials and Technology, Jiangsu Key Laboratory of Advanced Organic Materials, School of Chemistry and Chemical Engineering, Nanjing University, Nanjing, Jiangsu 210023, China*

Yandi Cai − *State Key Laboratory of Pollution Control and Resource Reuse, School of Environment, Jiangsu Key Laboratory of Vehicle Emissions Control, Center of Modern Analysis, Key Laboratory of Mesoscopic Chemistry of MOE, School of Chemistry and Chemical Engineering, Nanjing University, Nanjing 210023, China*

Qinglong Liu − *State Key Laboratory of Pollution Control and Resource Reuse, School of Environment, Jiangsu Key Laboratory of Vehicle Emissions Control, Center of Modern Analysis, Key Laboratory of Mesoscopic Chemistry of MOE, School of Chemistry and Chemical Engineering, Nanjing University, Nanjing 210023, China*

Kaiqiang Wu − *Jiangsu Key Laboratory of Atmospheric Environment Monitoring and Pollution Control (AEMPC), Jiangsu Collaborative Innovation Center of Atmospheric Environment and Equipment Technology (CICAEET), School of Environmental Science and Engineering, Nanjing University of Information Science and Technology, Nanjing 210044, China*

Dawei Li − *Jiangsu Key Laboratory of Atmospheric Environment Monitoring and Pollution Control (AEMPC), Jiangsu Collaborative Innovation Center of Atmospheric Environment and Equipment Technology (CICAEET), School of Environmental Science and Engineering, Nanjing University of Information Science and Technology, Nanjing 210044, China*

Lin Dong − *State Key Laboratory of Pollution Control and Resource Reuse, School of Environment, Jiangsu Key Laboratory of Vehicle Emissions Control, Center of Modern Analysis, Key Laboratory of Mesoscopic Chemistry of MOE, School of Chemistry and Chemical Engineering, Nanjing University, Nanjing 210023, China;* orcid.org/0000-0002-8393-6669

Complete contact information is available at: https://pubs.acs.org/10.1021/acs.inorgchem.4c04482

Notes

The authors declare no competing financial interest.

https://doi.org/10.1021/acs.inorgchem.4c04482
Inorg. Chem. XXXX, XXX, XXX−XXX

■ ACKNOWLEDGMENTS

W. T. thanks the support from National Natural Science Foundation of China (22306090), Natural Science Foundation of Jiangsu Province (BK20230773), Young Elite Scientists Sponsorship Program by CAST (No.YESS20230298), China Postdoctoral Science Foundation (2024M751391, GZB20240304) and Jiangsu Funding Program for Excellent Postdoctoral Talent (2024ZB828). L. D. thanks the support from the National Natural Science Foundation of China (22272077) and Natural Science Foundation of Jiangsu Province (BK20231513). D. L. thanks the support from the National Natural Science Foundation of China (52000101). F. L. thanks the Startup Fund from the University of California, Riverside (UCR).

■ REFERENCES

(1) Li, P.; Zhang, R.; Liu, N.; Royer, S. Efficiency of Cu and Pd substitution in Fe-based perovskites to promote N_2 formation during NH_3 selective catalytic oxidation (NH_3-SCO). *Appl. Catal., B* **2017**, *203*, 174−188.

(2) Campisi, S.; Palliggiano, S.; Gervasini, A.; Evangelisti, C. Finely Iron-Dispersed Particles on β Zeolite from Solvated Iron Atoms: Promising Catalysts for NH_3-SCO. *J. Phys. Chem. C* **2019**, *123* (18), 11723−11733.

(3) Xu, G.; Zhang, Q.; Yao, Y.; Zhang, X. Changes in $PM_{2.5}$ sensitivity to NO_x and NH_3 emissions due to a large decrease in SO_2 emissions from 2013 to 2018. *Atmosph. Oceanic Sci. Lett.* **2020**, *13* (3), 210−215.

(4) Liu, W.; Long, Y.; Tong, X.; Yin, Y.; Li, X.; Hu, J. Transition metals modified commercial SCR catalysts as efficient catalysts in NH_3-SCO and NH_3-SCR reactions. *Mol. Catal.* **2021**, *515*, 111888.

(5) Yu, Y.; Wei, D.; Tong, Z.; Wang, J.; Chen, J.; He, C. Rationally engineered ReO_x-$CuSO_4/TiO_2$ catalyst with superior NH_3-SCO efficiency and remarkably boosted SO_2 tolerance: Synergy of acid sites and surface adsorbed oxygen. *Chem. Eng. J.* **2022**, *442*, 136356.

(6) Park, S.-J.; Jin, S.-Y. Effect of ozone treatment on ammonia removal of activated carbons. *J. Colloid Interface Sci.* **2005**, *286* (1), 417−419.

(7) Behera, S. N.; Sharma, M.; Aneja, V. P.; Balasubramanian, R. Ammonia in the atmosphere: A review on emission sources, atmospheric chemistry and deposition on terrestrial bodies. *Environ. Sci. Pollut. Res.* **2013**, *20*, 8092−8131.

(8) Jabłońska, M.; Palkovits, R. Copper based catalysts for the selective ammonia oxidation into nitrogen and water vapour—Recent trends and open challenges. *Appl. Catal., B* **2016**, *181*, 332−351.

(9) Fenn, M. E.; Bytnerowicz, A.; Schilling, S. L.; Vallano, D. M.; Zavaleta, E. S.; Weiss, S. B.; Morozumi, C.; Geiser, L. H.; Hanks, K. On-road emissions of ammonia: An underappreciated source of atmospheric nitrogen deposition. *Sci. Total Environ.* **2018**, *625*, 909−919.

(10) Sun, K.; Tao, L.; Miller, D. J.; Pan, D.; Golston, L. M.; Zondlo, M. A.; Griffin, R. J.; Wallace, H. W.; Leong, Y. J.; Yang, M. M.; et al. Vehicle emissions as an important urban ammonia source in the United States and China. *Environ. Sci. Technol.* **2017**, *51* (4), 2472−2481.

(11) Huang, Y.; Liu, S.; Pei, M.-M.; Li, J.-Y.; Xu, H.-D.; Chen, Y.-Q. Unveiling H_2O_2-optimized NO_x adsorption-selective catalytic reduction (AdSCR) performance of $WO_3/CeZrO_2$ catalyst. *Rare Met.* **2023**, *42* (11), 3755−3765.

(12) Ma, L.-W.; Xi, X.-L.; Chen, J.-P.; Guo, F.; Yang, Z.-J.; Nie, Z.-R. Comprehensive recovery of W, V, and Ti from spent selective reduction catalysts. *Rare Met.* **2023**, *42* (10), 3518−3531.

(13) Chang, S.; Harle, G.; Ma, J.; Yi, J. The effect of textural properties of CeO_2-SiO_2 mixed oxides on NH_3-SCO activity of Pt/CeO_2-SiO_2 catalyst. *Appl. Catal., A* **2020**, *604*, 117775.

(14) Jabłońska, M. Progress on Noble Metal-Based Catalysts Dedicated to the Selective Catalytic Ammonia Oxidation into Nitrogen and Water Vapor (NH3-SCO). *Molecules* **2021**, *26* (21), 6461.

(15) Zhang, Q.; Wang, H.; Ning, P.; Song, Z.; Liu, X.; Duan, Y. In situ DRIFTS studies on CuO-Fe_2O_3 catalysts for low temperature selective catalytic oxidation of ammonia to nitrogen. *Appl. Surf. Sci.* **2017**, *419*, 733−743.

(16) Tskhovrebov, A. G.; Solari, E.; Wodrich, M. D.; Scopelliti, R.; Severin, K. Covalent Capture of Nitrous Oxide by N-Heterocyclic Carbenes. *Angew. Chem.* **2012**, *124* (1), 236−238.

(17) Zhu, M.; Lai, J.-K.; Wachs, I. E. Formation of N_2O greenhouse gas during SCR of NO with NH_3 by supported vanadium oxide catalysts. *Appl. Catal., B* **2018**, *224*, 836−840.

(18) Shin, Y.; Jung, Y.; Cho, C. P.; Pyo, Y. D.; Jang, J.; Kim, G.; Kim, T. M. NO_x abatement and N_2O formation over urea-SCR systems with zeolite supported Fe and Cu catalysts in a nonroad diesel engine. *Chem. Eng. J.* **2020**, *381*, 122751.

(19) Sun, M.; Zhou, S.; Wang, S.; Song, C. Optimized Design Method for Pt/SiO_2-Al_2O_3 with High NH_3-SCO Activity and Thermal Stability. *ACS Omega* **2022**, *7* (4), 3177−3184.

(20) Wang, H.; Murayama, T.; Lin, M.; Sakaguchi, N.; Haruta, M.; Miura, H.; Shishido, T. Understanding the Distinct Effects of Ag Nanoparticles and Highly Dispersed Ag Species on N_2 Selectivity in NH_3−SCO Reaction. *ACS Catal.* **2022**, *12* (10), 6108−6118.

(21) Sun, M.; Liu, J.; Song, C.; Ogata, Y.; Rao, H.; Zhao, X.; Xu, H.; Chen, Y. Different Reaction Mechanisms of Ammonia Oxidation Reaction on Pt/Al_2O_3 and Pt/$CeZrO_2$ with Various Pt States. *ACS Appl. Mater. Interfaces* **2019**, *11* (26), 23102−23111.

(22) Wang, F.; Ma, J.; He, G.; Chen, M.; Zhang, C.; He, H. Nanosize Effect of Al_2O_3 in Ag/Al_2O_3 Catalyst for the Selective Catalytic Oxidation of Ammonia. *ACS Catal.* **2018**, *8* (4), 2670−2682.

(23) Mieher, W.; Ho, W. Thermally activated oxidation of NH_3 on Pt(111): Intermediate species and reaction mechanisms. *Surf. Sci.* **1995**, *322* (1−3), 151−167.

(24) Svintsitskiy, D. A.; Kibis, L. S.; Stadnichenko, A. I.; Slavinskaya, E. M.; Romanenko, A. V.; Fedorova, E. A.; Stonkus, O. A.; Doronkin, D. E.; Marchuk, V.; Zimina, A.; Casapu, M. Insight into the nature of active species of Pt/Al_2O_3 catalysts for low temperature NH_3 oxidation. *ChemCatchem* **2020**, *12* (3), 867−880.

(25) Slavinskaya, E. M.; Kibis, L. S.; Stonkus, O. A.; Svintsitskiy, D. A.; Stadnichenko, A. I.; Fedorova, E. A.; Romanenko, A. V.; Marchuk, V.; Doronkin, D. E.; Boronin, A. I. The effects of platinum dispersion and Pt state on catalytic properties of Pt/Al_2O_3 in NH_3 oxidation. *ChemCatchem* **2021**, *13* (1), 313−327.

(26) Wang, H.; Lin, M.; Murayama, T.; Feng, S.; Haruta, M.; Miura, H.; Shishido, T. Selective catalytic oxidation of ammonia to nitrogen over zeolite-supported Pt-Au catalysts: Effects of alloy formation and acid sites. *J. Catal.* **2021**, *402*, 101−113.

(27) Tan, W.; Xie, S.; Le, D.; Diao, W.; Wang, M.; Low, K.-B.; Austin, D.; Hong, S.; Gao, F.; Dong, L.; Ma, L. Fine-tuned local coordination environment of Pt single atoms on ceria controls catalytic reactivity. *Nat. Commun.* **2022**, *13* (1), 7070.

(28) Liu, J.; Xu, G.; An, Q.; Wang, Y.; Yu, Y.; He, H. Heat Treatment Improves the Activity and Water Tolerance of Pt/Al_2O_3 Catalysts in Ammonia Catalytic Oxidation. *ACS Omega* **2023**, *8* (15), 13944−13954.

(29) Sharma, L.; Purdy, S. C.; Page, K.; Rangarajan, S.; Pham, H.; Datye, A.; Baltrusaitis, J. Sulfur Tolerant Subnanometer Fe/Alumina Catalysts for Propane Dehydrogenation. *ACS Appl. Nano Mater.* **2021**, *4* (10), 10055−10067.

(30) Zhang, W.; Shi, X.; Yan, Z.; Shan, Y.; Zhu, Y.; Yu, Y.; He, H. Design of High-Performance Iron−Niobium Composite Oxide Catalysts for NH_3-SCR: Insights into the Interaction between Fe and Nb. *ACS Catal.* **2021**, *11* (15), 9825−9836.

(31) Yu, D.; Wang, P.; Li, X.; Zhao, H.; Lv, X. Study on the role of Fe species and acid sites in NH_3-SCR over the Fe-based zeolites. *Fuel* **2023**, *336*, 126759.

https://doi.org/10.1021/acs.inorgchem.4c04482
Inorg. Chem. XXXX, XXX, XXX−XXX

(32) Long, R. Q.; Yang, R. T. Selective Catalytic Oxidation of Ammonia to Nitrogen over Fe_2O_3−TiO_2 Prepared with a Sol−Gel Method. *J. Catal.* **2002**, *207* (2), 158−165.
(33) Wang, H.-M.; Ning, P.; Zhang, Q.-L.; Liu, X.; Zhang, T.-X.; Hu, J.; Wang, L.-Y. Effect of different RuO_2 contents on selective catalytic oxidation of ammonia over RuO_2-Fe_2O_3 catalysts. *J. Fuel Chem. Technol.* **2019**, *47* (2), 215−223.
(34) Hinokuma, S.; Shimanoe, H.; Matsuki, S.; Kawano, M.; Kawabata, Y.; Machida, M. Catalytic Activity and Selectivities of Metal Oxides and Pt/Al_2O_3 for NH_3 Combustion. *Chem. Lett.* **2016**, *45* (2), 179−181.
(35) Wang, F.; Zhu, Y.; Li, Z.; Shan, Y.; Shan, W.; Shi, X.; Yu, Y.; Zhang, C.; Li, K.; Ning, P. Promoting effect of acid sites on NH_3-SCO activity with water vapor participation for Pt-Fe/ZSM-5 catalyst. *Catal. Today* **2021**, *376*, 311−317.
(36) Gu, Z.; Tan, C.; Zhu, B.; Sin, S.; Ji, J.; Wang, Y.; Cheng, L.; Song, W.; Huang, C.; Tao, M.; Tang, C. SO_4^{2-} immobilization regulated by reaction atmosphere over ABS poisoned α-Fe_2O_3 catalysts for efficient NO_x removal. *Chem. Eng. J.* **2023**, *475*, 146336.
(37) Li, Y.; Xiao, P.; Xiong, J.; Luo, J.; Zhou, P.; Xie, X.; Li, Y.; Chen, M. Scalable fabrication of nano/porous Fe-Si coated by 2D carbon nanosheets composite anode for high-performance lithium-ion batteries. *J. Alloys Compd.* **2023**, *945*, 169331.
(38) Sun, J.; Liu, X.; Zheng, P.; Zhao, Y.; Zheng, Y.; Chai, J.; Liu, Z. Mitigating the volume expansion and enhancing the cycling stability of ferrous fluorosilicate-modified silicon-based composite anodes for lithium-ion batteries. *J. Mater. Chem.* **2024**, *12* (38), 25747−25760.
(39) Hausmann, J. N.; Beltrán-Suito, R.; Mebs, S.; Hlukhyy, V.; Fässler, T. F.; Dau, H.; Driess, M.; Menezes, P. W. Evolving highly active oxidic iron (III) phase from corrosion of intermetallic iron silicide to master efficient electrocatalytic water oxidation and selective oxygenation of 5-hydroxymethylfurfural. *Adv. Mater.* **2021**, *33* (27), 2008823.
(40) Lee, S.; Seo, J.-C.; Chun, H.-J.; Yang, S.; Sim, E.-H.; Lee, J.; Kim, Y. T. Selective olefin production on silica based iron catalysts in Fischer−Tropsch synthesis. *Catal. Sci. Technol.* **2022**, *12* (19), 5814−5828.
(41) Han, Z.; Ying, W.; Zhang, H.; Ma, H.; Qian, W. Role of SiO_2 in different iron-based catalysts for Fischer−Tropsch synthesis to light olefins. *Fuel* **2023**, *338*, 127257.
(42) Yang, S.; Guo, Y.; Chang, H.; Ma, L.; Peng, Y.; Qu, Z.; Yan, N.; Wang, C.; Li, J. Novel effect of SO_2 on the SCR reaction over CeO_2: Mechanism and significance. *Appl. Catal., B* **2013**, *136*, 19−28.
(43) Gao, F.; Liu, Y.; Sani, Z.; Tang, X.; Yi, H.; Zhao, S.; Yu, Q.; Zhou, Y. Advances in selective catalytic oxidation of ammonia (NH_3−SCO) to dinitrogen in excess oxygen: A review on typical catalysts, catalytic performances and reaction mechanisms. *J. Environ. Chem. Eng.* **2021**, *9* (1), 104575.
(44) Shi, G.; Li, P.; Li, K.; Hu, F.; Liu, Q.; Zhou, H.; Liu, Z. Insight into NO_x formation characteristics of ammonia oxidation in N_2 and H_2O atmospheres. *Energy* **2023**, *285*, 129412.
(45) Lan, Y.; Li, X.; Li, G.; Luo, Y. Sol−gel method to prepare graphene/Fe2O3 aerogel and its catalytic application for the thermal decomposition of ammonium perchlorate. *J. Nanopart. Res.* **2015**, *17* (10), 395.
(46) Lester, E.; Hilal, N.; Henderson, J. Porosity in ancient glass from Syria (c. 800 AD) using gas adsorption and atomic force microscopy. *Surf. Interface Anal.* **2004**, *36* (9), 1323−1329.
(47) Ahmed, A. E.; Adam, F. Indium incorporated silica from rice husk and its catalytic activity. *Microporous Mesoporous Mater.* **2007**, *103* (1−3), 284−295.
(48) Feifel, S. C.; Lisdat, F. Silica nanoparticles for the layer-by-layer assembly of fully electro-active cytochrome c multilayers. *J. Nanobiotechnol.* **2011**, *9* (1), 59.
(49) Tan, W.; Liu, A.; Xie, S.; Yan, Y.; Shaw, T. E.; Pu, Y.; Guo, K.; Li, L.; Yu, S.; Gao, F. Ce−Si Mixed Oxide: A High Sulfur Resistant Catalyst in the NH_3−SCR Reaction through the Mechanism-Enhanced Process. *Environ. Sci. Technol.* **2021**, *55* (6), 4017−4026.
(50) Qing, M.; Yang, Y.; Wu, B.; Xu, J.; Zhang, C.; Gao, P.; Li, Y. Modification of Fe−SiO_2 interaction with zirconia for iron-based Fischer−Tropsch catalysts. *J. Catal.* **2011**, *279* (1), 111−122.
(51) Yang, K.; Zhou, C.; Li, C.; Dou, S.; Li, X.; Wang, X.; Xu, X. Efficient removal of Sb(V) in textile wastewater through novel amorphous Si-doped Fe oxide composites: Phase composition, stability and adsorption mechanism. *Chem. Eng. J.* **2021**, *407*, 127217.
(52) Tan, W.; Xie, S.; Shan, W.; Lian, Z.; Xie, L.; Liu, A.; Gao, F.; Dong, L.; He, H.; Liu, F. CeO_2 doping boosted low-temperature NH_3-SCR activity of $FeTiO_x$ catalyst: A microstructure analysis and reaction mechanistic study. *Front. Environ. Sci. Eng.* **2022**, *16* (5), 60.
(53) Zhang, B.-L.; Deng, L.-F.; Liu, B.; Luo, C.-Y.; Liebau, M.; Zhang, S.-G.; Gläser, R. Synergistic effect of cobalt and niobium in Co_3-Nb-O_x on performance of selective catalytic reduction of NO with NH_3. *Rare Met.* **2022**, *41* (1), 166−178.
(54) Xu, Y.; Wang, P.; Pu, Y.; Jiang, L.; Yang, L.; Jiang, W.; Yao, L. MnCe/GAC-CNTs catalyst with high activity, SO_2 and H_2O tolerance for low-temperature NH_3-SCR. *Sep. Purif. Technol.* **2023**, *305*, 122498.
(55) Wang, Z.; Qu, Z.; Quan, X.; Li, Z.; Wang, H.; Fan, R. Selective catalytic oxidation of ammonia to nitrogen over CuO-CeO_2 mixed oxides prepared by surfactant-templated method. *Appl. Catal., B* **2013**, *134*−*135*, 153−166.
(56) Qu, Z.; Wang, H.; Wang, S.; Cheng, H.; Qin, Y.; Wang, Z. Role of the support on the behavior of Ag-based catalysts for NH_3 selective catalytic oxidation (NH_3-SCO). *Appl. Surf. Sci.* **2014**, *316*, 373−379.
(57) Yu, Y.; Tan, W.; An, D.; Tang, C.; Zou, W.; Ge, C.; Tong, Q.; Gao, F.; Sun, J.; Dong, L. Activity enhancement of WO_3 modified $FeTiO_x$ catalysts for the selective catalytic reduction of NO_x by NH_3. *Catal. Today* **2021**, *375*, 614−622.
(58) Ren, Z.; Zhang, H.; Huang, J.; Chen, H.; Wang, G.; Long, H.; Yu, Z.; Su, Z.; Zhang, Y. Investigation of RuO_x doping stimulated the high catalytic activity of CeO_x-MnO_x/TiO_2 catalysts in the NH_3-SCR reaction: Structure-activity relationship and reaction mechanism. *J. Alloys Compd.* **2022**, *910*, 164814.
(59) Ren, Z.; Zhang, H.; Wang, G.; Pan, Y.; Yu, Z.; Long, H. Effect of Calcination Temperature on the Activation Performance and Reaction Mechanism of Ce−Mn−Ru/TiO_2 Catalysts for Selective Catalytic Reduction of NO with NH_3. *ACS Omega* **2020**, *5* (51), 33357−33371.
(60) Chen, L.; Li, J.; Ge, M. DRIFT Study on Cerium− Tungsten/Titiania Catalyst for Selective Catalytic Reduction of NO_x with NH_3. *Environ. Sci. Technol.* **2010**, *44* (24), 9590−9596.
(61) Guo, X.-H.; Sun, S.-Y.; Gao, M.-X.-Z.; Dai, Q.-G.; Zhan, W.-C.; Wang, L.; Guo, Y.; Wang, A.-Y.; Guo, Y.-L. Highly efficient Ag/Ce−Zr catalyst for catalytic oxidation of NVOCs: Balance of redox ability and acidity. *Rare Met.* **2024**, *43* (12), 6473−6485.
(62) Chen, L.; Li, J.; Ge, M. DRIFT Study on Cerium−Tungsten/Titiania Catalyst for Selective Catalytic Reduction of NO_x with NH_3. *Environ. Sci. Technol.* **2010**, *44* (24), 9590−9596.
(63) Wei, L.; Li, X.; Mu, J.; Wang, X.; Fan, S.; Yin, Z.; Tadé, M. O.; Liu, S. Rationally Tailored Redox Properties of a Mesoporous Mn−Fe Spinel Nanostructure for Boosting Low-Temperature Selective Catalytic Reduction of NO_x with NH_3. *ACS Sustainable Chem. Eng.* **2020**, *8* (48), 17727−17739.
(64) Zhao, P.; Guo, M.; Liu, Q.; Fan, L.; Han, J.; Liu, C.; Ji, N.; Song, C.; Ma, D.; Li, Z. Novel $Mn_aZr_bCr_cO_x$ catalysts for low temperature NH_3-SCR derived from high H_2O content flue gas via natural gas combustion. *Chem. Eng. J.* **2019**, *378*, 122100.
(65) Zhang, N.; Li, L.; Guo, Y.; He, J.; Wu, R.; Song, L.; Zhang, G.; Zhao, J.; Wang, D.; He, H. A MnO_2-based catalyst with H_2O resistance for NH_3-SCR: Study of catalytic activity and reactants-H_2O competitive adsorption. *Appl. Catal., B* **2020**, *270*, 118860.
(66) Tan, Y.; Li, F.; Zhao, B.; Chen, W.; Tian, M. Hydrothermal Synthesis of a Ce−Zr−Ti Mixed Oxide Catalyst with Enhanced Catalytic Performance for a NH_3-SCR Reaction. *Langmuir* **2021**, *37* (51), 14823−14832.
(67) Li, Z.; Wang, C.; Qiu, J.; Ma, Y.; Wang, C.; Sun, X.; Li, K.; Ning, P.; Wang, F. Advances in selective catalytic oxidation of

https://doi.org/10.1021/acs.inorgchem.4c04482
Inorg. Chem. XXXX, XXX, XXX−XXX

ammonia (NH_3-SCO): A review of catalyst structure-activity relationship and design principles. *Chin. Chem. Lett.* **2024**, *35*, 108432.
(68) Lan, T.; Zhao, Y.; Deng, J.; Zhang, J.; Shi, L.; Zhang, D. Selective catalytic oxidation of NH_3 over noble metal-based catalysts: state of the art and future prospects. *Catal. Sci. Technol.* **2020**, *10* (17), 5792−5810.
(69) Peng, Y.; Liu, C.; Zhang, X.; Li, J. The effect of SiO_2 on a novel CeO_2−WO_3/TiO_2 catalyst for the selective catalytic reduction of NO with NH_3. *Appl. Catal., B* **2013**, *140*−*141*, 276−282.
(70) Yu, Y.; Chen, C.; Ma, M.; Douthwaite, M.; He, C.; Miao, J.; Chen, J.; Li, C. SO_2 promoted in situ recovery of thermally deactivated $Fe_2(SO_4)_3$/TiO_2 NH_3-SCR catalysts: From experimental work to theoretical study. *Chem. Eng. J.* **2019**, *361*, 820−829.
(71) Song, L.; Yue, H.; Ma, K.; Tian, W.; Liu, W.; Liu, C.; Tang, S.; Liang, B. Mechanistic Aspects of Highly Efficient $Fe_aS_bTiO_x$ Catalysts for the NH_3-SCR Reaction: Insight into the Synergistic Effect of Fe and S Species. *Ind. Eng. Chem. Res.* **2020**, *59* (17), 8164−8173.
(72) Xie, H.; Shu, D.; Chen, T.; Liu, H.; Zou, X.; Wang, C.; Han, Z.; Chen, D. An *in-situ* DRIFTs study of Mn doped $FeVO_4$ catalyst by one-pot synthesis for low-temperature NH_3-SCR. *Fuel* **2022**, *309*, 122108.
(73) Xue, H.; Guo, X.; Meng, T.; Mao, D.; Ma, Z. NH_3-SCR of NO over M/ZSM-5 (M = Mn, Co, Cu) catalysts: An *in-situ* DRIFTS study. *Surf. Interfaces* **2022**, *29*, 101722.
(74) Li, Z.; Gao, M.; Lv, Z.; Duan, R.; Shan, Y.; Li, H.; He, G.; He, H. Uncovering the Dinuclear Mechanism of NO_2-Involved NH_3−SCR over Supported V_2O_5/TiO_2 Catalysts. *Environ. Sci. Technol.* **2023**, *57* (45), 17577−17587.
(75) Lin, M.; An, B.; Niimi, N.; Jikihara, Y.; Nakayama, T.; Honma, T.; Takei, T.; Shishido, T.; Ishida, T.; Haruta, M. Role of the Acid Site for Selective Catalytic Oxidation of NH_3 over Au/Nb_2O_5. *ACS Catal.* **2019**, *9* (3), 1753−1756.
(76) Yao, P.; Li, J.; Pei, M.; Liu, F.; Xu, H.; Chen, Y. Engineering a PtCu Alloy to Improve N_2 Selectivity of NH_3−SCO over the Pt/SSZ-13 Catalyst. *ACS Appl. Mater. Interfaces* **2024**, *16* (12), 14694−14703.
(77) Lin, Q.-J.; Pei, M.-M.; Yao, P.; Xu, S.; Xu, S.-H.; Liu, S.; Xu, H.-D.; Dan, Y.; Chen, Y.-Q. Determining hydrothermal deactivation mechanisms on Cu/SAPO-34 NH_3-SCR catalysts at low-and high-reaction regions: Establishing roles of different reaction sites. *Rare Met.* **2022**, *41* (6), 1899−1910.
(78) Kumar, P. A.; Jeong, Y. E.; Gautam, S.; Ha, H. P.; Lee, K. J.; Chae, K. H. XANES and DRIFTS study of sulfated Sb/V/Ce/TiO_2 catalysts for NH_3-SCR. *Chem. Eng. J.* **2015**, *275*, 142−151.
(79) Wang, X.; Li, B.; Wang, Y.; Wei, T.; Li, S.; Li, W. Insight into the dynamic behaviors of reactants with temperature over a TiO_x-based catalyst for NO_x removal via NH_3-SCR. *Appl. Surf. Sci.* **2022**, *605*, 154689.

https://doi.org/10.1021/acs.inorgchem.4c04482
Inorg. Chem. XXXX, XXX, XXX−XXX